DETERMINATION OF WAVE SLAMMING LOADS ON HIGH-SPEED CATAMARANS BY HYDROELASTIC SEGMENTED MODEL EXPERIMENTS

J Lavroff, M R Davis, D S Holloway and **G Thomas**, University of Tasmania, Australia.
(DOI No: 10.3940/rina.ijme.2011.a3.211)

SUMMARY

A 2.5m hydroelastic segmented catamaran model has been developed based on the 112m INCAT wave-piercer catamaran to simulate the vibration response during the measurement of dynamic slam loads in head seas. Towing tank tests were performed in regular seas to measure the dynamic slam loads acting on the centre bow and vertical bending moments acting in the demihulls of the catamaran model as a function of wave frequency and wave height to establish the operational loads acting on the full-scale 112m INCAT catamaran vessel. Peak slam forces measured on the bow of the model are found to approach the weight of the model, this being similar to the findings of full-scale vessel trials. A review of the motions of the hydroelastic segmented catamaran model found that the heave and pitch motions give a good indication of slamming severity in terms of the dimensionless heave and pitch accelerations. The dynamic wave slam forces are closely related to the relative motion between the bow and the incident wave profile.

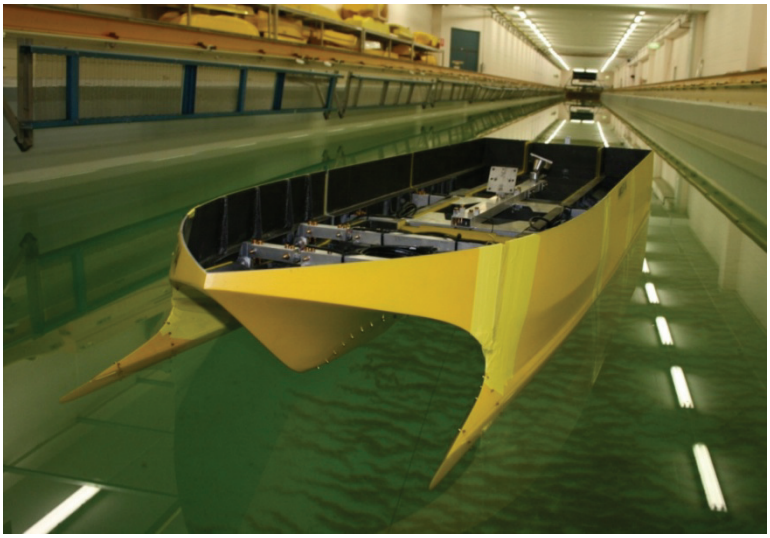

Figure 1: Hydroelastic segmented catamaran model of the 112m INCAT wave-piercer catamaran.

NOMENCLATURE

c = Distance of slam force on transverse beam from centreline of port demihull pin joint mount (m)
F = Peak sagging slam force (N)
F_i' = Slam force acting on centre bow transverse beam (N)
F_1' = Slam force acting on centre bow forward transverse beam (N)
F_2' = Slam force acting on centre bow aft transverse beam (N)
F_T' = Total slam force acting on centre bow mounted on transverse beams (N)
g = Gravity (m s^{-2})
H^* = Heave amplitude/wave amplitude
L = Overall length of model (m)
l_1 = Distance between centreline of demihull pin joint mount and centre of elastic hinge (m)
l_2 = Distance between strain gauges mounted on port elastic hinge and starboard elastic hinge of centre bow transverse beam (m)
M = Bending moment (Nm)
M_1' = Moment acting on port elastic hinge of centre bow transverse beam (Nm)
M_2' = Moment acting on starboard elastic hinge of centre bow transverse beam (Nm)
m = Model mass (kg)
P^* = Pitch amplitude/maximum wave slope
t_i = Time reference points (s)
w_2 = Distance between centrelines of centre bow forward and aft transverse beams (m)
x_1 = Position of total slam force acting on centre bow in transverse beam configuration

measured from the centreline of the aft transverse beam (m)

ς = Wave amplitude (m)

ρ = Density of water (kg m^{-3})

ω_e = Wave encounter frequency (rad s^{-1})

ω_e^* = Dimensionless wave encounter frequency $= \omega_e \sqrt{l/g}$, where l = waterline length

1. INTRODUCTION

Global demand for high-speed transportation has led to the on-going development of high-speed catamarans and high-speed monohulls for both commercial and military applications. Commercial applications have traditionally involved the transport of passengers and vehicles along commercial ferry routes while more recently the use of high-speed vessels has been extended to military applications to exploit the capability of transporting vehicles and equipment with significantly reduced travel times.

The most common design used by ship builders is the catamaran vessel, consisting of a central flat wet-deck section and the two demihulls. This type of design is effective during operation in smaller waves. However, in larger waves this type of catamaran vessel is prone to deck diving causing the wet-deck to encounter the wave surface resulting in water passing over the bow. The slam impact of the water surface on the underside of the wet-deck imparts an impulsive slam load on the structure resulting in instantaneous impulsive longitudinal bending flexure and a whipping vibration response [1, 2, 3]. While designers strive to improve the performance of high-speed vessels using light-weight materials and optimal design processes, wet-deck slamming in large seas has been known to cause structural damage to the bows and hulls of high-speed vessels [4].

Although deck diving and wave slamming of multi-hull vessels can cause extreme wave slam loads, the rate of deck diving and severity of slamming can be significantly reduced with the introduction of a centre bow as in the design of INCAT wave-piercer catamaran vessels. The centre bow acts to provide forward buoyancy to the front of the vessel during wave entry of the bow, but due to slam impact between the centre bow and demihulls the ship structure is still subject to extreme dynamic structural loads that are not easily predicted by analysis owing to the complicated three dimensional unsteady nature of the hull-water interaction. Although there exists knowledge on the different types of slamming that affect monohulls, such as bow flare slamming [5, 6] and aft body slamming [7], the incidence and severity of slamming on high-speed multi-hull vessels, in particular with a centre bow, still remains subject to on-going research [8].

Numerical techniques developed by Holloway and Davis, [9], have been extended to predict the dynamic structural loads acting on high-speed slender hull forms in regular seas and give generally good agreement with the results of finite element methods used in combination with strain gauge data collected during full-scale vessel trials [10]. The instrumentation of full-scale catamaran vessels also provided the basis for the investigation of dynamic structural loads, in particular the non-linear wave slam forces acting on the centre bow and whipping vibration responses, [11]. Strain gauge data collected during full-scale vessel trials performed on an 86m INCAT hull was used on a quasi-static basis and also in a dynamic finite element analysis to evaluate the slam force of an extreme and damaging wave slam event, [12]. The results of the dynamic finite element analysis identified a maximum slam force of 1025 tonnes on the forward starboard side of the catamaran vessel causing significant damage to the aluminium shell structure. The research results of this work thus identified the potentially large magnitude of the wave slam loads. This showed the importance of undertaking further research to develop a more accurate understanding of the parameters influencing the wave induced slam force and wave slam occurrence. In particular, it is not clear whether the maximum slam force observed during sea trials represented the maximum possible or extreme slam force. Also, this most severe recorded slam event took place at a relatively low speed and it was not clear whether more severe slams can occur at higher speeds. One aim of the present work is to carry out controlled model tests in order to determine the extreme loads which can occur. However, since the experience at full scale has been that severe slams occur at moderate speeds the tests to be described in this paper deal with slamming at the equivalent of 20 knots at full scale, a commonly adopted reduced speed when vessels capable of 40 knots encounter significant head seas and so reduce speed to moderate the effects of wave encounter.

The continued demand for increasing payload capacity recently resulted in the production of the 112m INCAT catamaran (www.incat.com.au) capable of reaching speeds up to 40 knots at a loaded ship displacement of 2500 tonne, or 3000 tonne at reduced speed. The significant increase in size and weight compared to previous wave-piercing catamaran vessels increases the need to develop analytical methods for the prediction of the non-linear wave induced slam forces and slam induced bending moments. Although high-speed catamaran vessels may be subject to encounter many slam cycles during their service life, relatively little is known regarding the parameters controlling the slam loads and methods of analysis available for predicting the magnitude of the slam force are presently not adequate. It has been found that prediction methods based on two dimensional model testing or computation substantially over-predicts the magnitude of slam loads

by as much as three times [13, 14]. Moreover, the subsequent whipping vibration responses commonly observed on high-speed vessels [3, 6] present an additional factor that needs to be considered especially in the prediction of the dynamic structural loads as discussed by Faltinsen [15] and Bereznitski [16] and of vessel fatigue.

Three-dimensional model tests have demonstrated the potential for measuring dynamic wave loads at model scale in controlled wave conditions for the purposes of evaluating the structural loads and simulating the whipping vibration responses. Hermundstad et al. [17, 18] developed a high Froude number hydroelastic segmented catamaran model (4.1 m length and 203 kg mass) to measure the motions and loads in controlled wave conditions. Although extensive research has seen the development of hydroelastic models for the measurement and numerical validation of motions, bending moments and whipping vibration responses [19], there is little information available on the processes which determine slam occurrence and in particular, the magnitude of the wave induced slam force acting on the centre bow of high-speed wave-piercing catamaran vessels.

During the course of the current investigation, towing tank tests of a hydroelastic segmented catamaran model were performed in regular seas at the Australian Maritime College towing tank (www.amc.edu.au) to investigate the parameters affecting the slamming and whipping vibratory responses [20] as a function of wave height and wave encounter frequency. The hydroelastic model set-up and calibration procedures will be described in this paper and the towing tank test program and test procedures are to be explained. Raw strain gauge data obtained from the towing tank tests is analysed and quasi-static procedures are used to calculate the slam loads on the bow and the slam induced bending moments in the demihull.

2. HYDROELASTIC SEGMENTED CATAMARAN MODEL SET-UP

The 112m INCAT Tasmania catamaran was used as a basis for designing the geometrically similar 2.5m hydroelastic segmented catamaran model. The segmented model concept followed the approach of the model designs previously adopted by McTaggart et al. [19], Dessi et al. [21] and Hermundstad et al. [18, 22]. Figure 1 shows a photograph of the model at the Australian Maritime College towing tank and Figure 2 shows a layout plan of the model. Table 1 shows the main particulars of the model.

The segmented model demihulls were separated at two locations along the demihull axis to create three rigid hull segments. The centre bow of the model was constructed as a separate segment so as to isolate the slam loads acting on the bow. This configuration allowed for the measurement of slam loads acting on the centre bow by a force balance analysis from the bending moments in the four elastic hinges mounted in the two transverse beams supporting the centre bow (Figure 3). In addition, vertical bending moments acting within the demihulls were measured at the locations of the elastic hinges connecting the demihull segments. The catamaran model hull segments were constructed from carbon fibre and Divinicell foam sandwich construction to produce a stiff and lightweight shell structure. An aluminium backbone beam was located within each rigid hull segment and the rigid segments were joined together by elastic hinges or bending springs, formed by short solid beams of aluminium. These elastic hinges were fitted with strain gauges on top and bottom surfaces connected to opposite sides of a strain gauge bridge for the measurement of wave induced bending loads. The demihull elastic hinges were designed to be interchangeable to allow for the variation of bending stiffness and thus making possible adjustment of the first longitudinal modal response frequency [20].

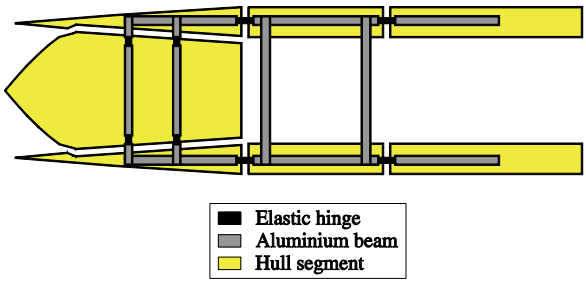

Figure 2: Layout plan of the 2.5m hydroelastic segmented catamaran model.

Table 1: Main particulars of the segmented catamaran model.

Description	Specification
Length overall	2.5m
Waterline length	2.3m
Overall beam of model	0.68m
Overall beam of demihull	0.129m
Displacement	27.43kg
Longitudinal centre of gravity (from aft perpendicular)	0.948m
Vertical centre of gravity (from keel)	0.091m
Pitch radius of gyration	0.64m

The slam force acting on the centre bow of the model was distributed between the two centre bow transverse mounting beams. The elastic hinges in the transverse beams were of a stiffness which placed the frequency of vibration of the centre bow on the transverse beams well beyond the frequency range of interest to ship simulation by a factor of about three. The port and starboard midship demihull segments were joined by rigid transverse beams to form a single rigid mid ship

section, this providing an effective mounting base for the forward and aft model towing posts.

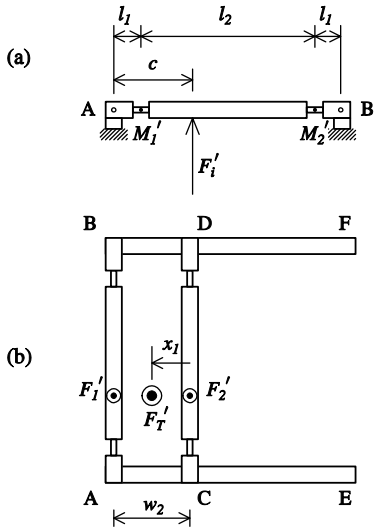

Figure 3: Centre bow transverse beam configuration for the evaluation of wave slamming loads: (a) Elevation of transverse beam, (b) Plan of forward and aft transverse beams (AB, CD), pin mounted on the demihull backbone beams (ACE, BDF).

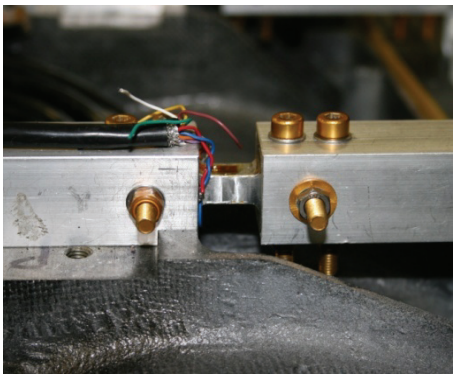

Figure 4: Centre bow transverse beam elastic hinge instrumented with strain gauges on top and bottom surfaces for the measurement of wave induced bending moments and the determination of slam forces.

Figure 3(a) shows a schematic elevation of the slam force acting on the centre bow transverse beam. The transverse beam consisted of a SHS aluminium tube pin mounted at both ends A and B to the demihull backbone beams and with elastic hinges located on the port and starboard sides at locations M_1' and M_2'. The pin mountings at positions A and B were fixed to the port and starboard demihull longitudinal beams respectively so as to transmit no bending moment, this forming the basis for determination of the total force and its location on the centre bow. Strain gauges were mounted on the top and bottom surfaces of each elastic hinge beam element (Figure 4): the elastic hinge elements were separated by a distance l_2. The port and starboard strain gauge measurement positions were located at a distance l_1 from pinned joints at A and B. Slam induced strains were measured at each of the elastic hinges making possible the evaluation of bending moments M_1' and M_2'. The slam force F_i', was then determined from the magnitudes and known positions of the measured bending moments. The position of the slam force c, was a function of these measured quantities.

The force balance equations for the centre bow then lead to the following results if inertia loads on the bow are neglected:

$$F_i' = \frac{M_1' + M_2'}{l_1} \tag{1}$$

$$c = \frac{M_2'(2l_1 + l_2)}{M_1' + M_2'} \tag{2}$$

The effect of the inertia of the centre bow was investigated in order to determine the influence of the bow inertia on the calculated slam force from strains measured during slam impact. Accelerations were measured using an Endevco accelerometer mounted on the centreline of the centre bow forward transverse beam during towing tank tests performed in regular seas to identify the maximum accelerations acting on the centre bow during peak slam impact. The peak accelerations measured on the model were then used to evaluate the inertia load of the centre bow so as to evaluate the accuracy of the (quasi-static) slam load calculation. Based on the accelerometer measurements, the calculated bow inertia force was found to be at most 17% of the calculated total peak sagging slam load. Thus the actual hydrodynamic slam load acting on the external bow surfaces might exceed the values reported here at most by 17% [21]. However, accelerometer records are not available for all tests, and so bow loads calculated from the transverse beam elastic link strain gauges neglecting the bow inertia loads are presented in this paper. Bearing in mind the generally approximate nature of model tests of this type and the considerable increase in complexity of data analysis required to correct for the centre bow inertia, it was considered acceptable to determine slamming forces on the centre bow using equations (1) and (2).

Figure 3(b) shows a schematic plan of the double transverse beam configuration for the evaluation of the total slam force acting on the centre bow. The forward transverse beam AB, and aft transverse beam CD, were pinned to the port and starboard demihull longitudinal beams ACE and BDF respectively. The demihull longitudinal beams were joined to the port and starboard mid-ship demihulls at locations E and F respectively. The forward and aft transverse beams were separated at width w_2. The total slam force acting on the centre bow F_T', was the summation of the forces

acting on the forward transverse beam F_1', and aft transverse beam F_2'. Thus the longitudinal position of the total slam force x_1, was calculated from the following results, where again the centre bow inertia is neglected:

$$F_T' = F_1 + F_2 \tag{3}$$

$$x_1 = \frac{F_1'}{F_1' + F_2'} w_2 \tag{4}$$

Experimental testing of the segmented catamaran model was conducted at the Australian Maritime College (AMC) in Launceston, Tasmania. The model testing was undertaken in head seas with a primary focus on measuring local and global catamaran loads and motions. As has been explained, the local slamming loads were measured on the centre bow and global wave induced vertical bending moments in each of the demihulls were determined on the basis of bending moments in the complete set of eight elastic hinges. Eight strain gauge bridges were connected to pairs of strain gauges mounted on each of the elastic hinges of the model so as to record the differential strain on the top and bottom surfaces of each elastic link beam element at each of the connection points along the catamaran model demihull and in the bow mounting transverse beams. The strain gauge bridge analog output signals were acquired at a sampling rate of 500 Hz by a National Instruments CompactRIO (cRIO) running Labview FPGA and recorded data was later transferred via Ethernet to a laptop computer running Labview.

Towing tank test models are attached to the moving carriage by tow posts mounted forward and aft of the model longitudinal centre of gravity (LCG). The towing carriage data acquisition and signal conditioning system separately recorded model motions and encountered wave data at a sampling rate of 100 Hz. Linear voltage displacement transducers (LVDTs) were mounted on each of the two tow posts and measured the vertical motions of each tow post to provide data for the calculation of model heave and pitch motions. A static wave probe was located at a fixed position near the towing tank wave maker and measured the wave height of the waves propagating forward from the wave maker. A resistance based wave probe was fixed to the towing tank carriage to measure the wave height at the longitudinal centre of gravity of the catamaran model. Instrumentation signals were amplified to an output of ±10.0 Volts per channel (reference single ended). The amplified analog signals were input to a PCM card digitiser from which the digital signal records were input to a desktop computer running Labview software. The LVDT data was synchronised with the cRIO strain gauge data using a common DC trigger that provided a 9 Volt DC step signal to both the cRIO and the towing tank data acquisition systems. The 9 Volt DC step signal activated the acquisition process on the cRIO and synchronised both the cRIO and towing tank data acquisition systems when the switch was released and the acquired voltage returned to zero.

3. CATAMARAN MODEL GLOBAL WAVE MOTIONS

The global wave motions of the hydroelastic segmented catamaran model were evaluated for all the tests performed to investigate the effect of the motions response on the peak dynamic structural loads. The LVDT data obtained from the towing tank data acquisition system was used to determine the heave and pitch motions response functions of the catamaran model. The response amplitude operators (RAOs) of the hydroelastic segmented catamaran model were then evaluated from the heave and pitch data based on taking the root mean square (RMS) of the heave and pitch signals. The RAOs were further evaluated based on identifying the peaks in the heave and pitch signals to determine the average amplitude of the response, however, Labview software limitations were encountered in accurately identifying the peaks due to slam impulse effects evident between the peaks and troughs of the sinusoidal heave response signal (Figures 5 – 6). Although slam impulse effects are clearly evident between the peaks and troughs of the sinusoidal heave response signal, the pitch motion response showed little evidence of slamming (Figures 7 – 8). On this basis the RAO functions presented here were calculated using the RMS method, this being identified as a more appropriate method of analysis [23].

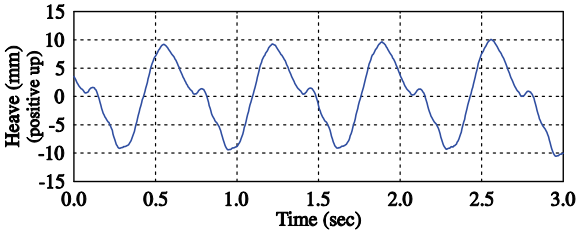

Figure 5: Hydroelastic segmented catamaran model heave response at a model test speed of 1.53m/s, wave height of 90mm and $\omega_e^* = 4.74$.

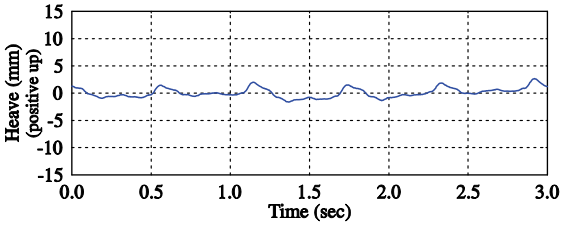

Figure 6: Hydroelastic segmented catamaran model heave response at a model test speed of 1.53m/s, wave height of 90mm and $\omega_e^* = 5.36$.

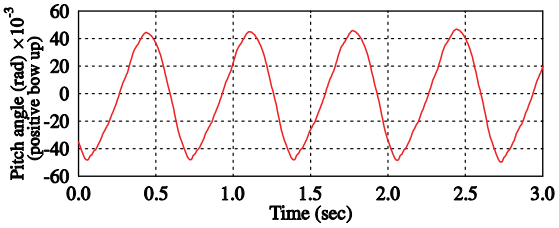

Figure 7: Hydroelastic segmented catamaran model pitch response at a model test speed of 1.53m/s, wave height of 90mm and $\omega_e^* = 4.74$.

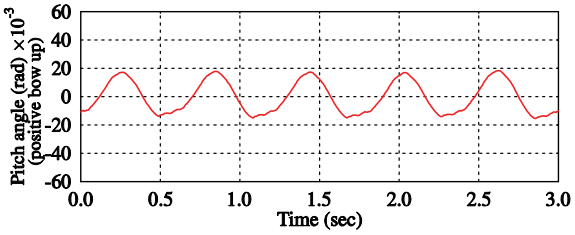

Figure 8: Hydroelastic segmented catamaran model pitch response at a model test speed of 1.53m/s, wave height of 90mm and $\omega_e^* = 5.36$.

It is evident from Figures 5 – 8 that increases in the dimensionless wave encounter frequency from 4.74 to 5.36 caused a significant reduction in both the heave and pitch response. The overall trend with wave encounter frequency is shown more clearly by the calculated RAO functions shown in Figures 9 and 10. In determining the heave response amplitude operators, the signal records more significantly affected by the slam impulse disturbances were for $\omega_e^* > 5.2$ (Figure 6). At these relatively high encounter frequencies the catamaran model motions were approaching very small response amplitude operator values.

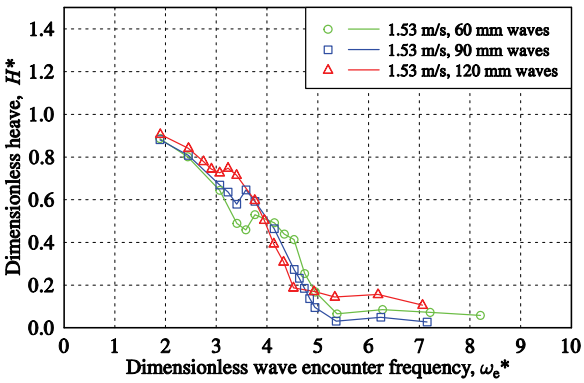

Figure 9: Hydroelastic segmented catamaran model dimensionless heave in head-seas at model test speed of 1.53m/s.

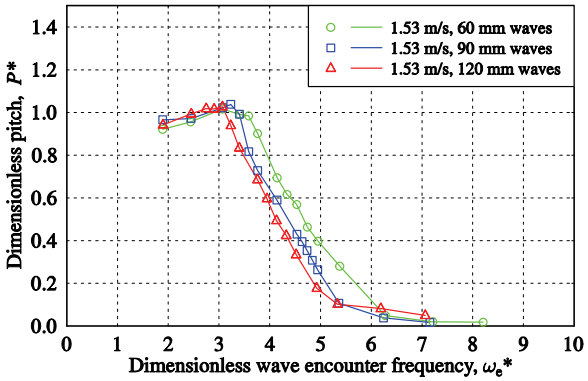

Figure 10: Hydroelastic segmented catamaran model dimensionless pitch in head-seas at model test speed of 1.53m/s.

We see from Figure 9, that for relatively low encounter frequencies the dimensionless heave was not significantly affected by the wave height. However, for dimensionless wave encounter frequencies ω_e^* between 2.4 and 3.6 heave motions are observed to increase in larger waves, whilst for ω_e^* values between 4 and 4.6, heave motions decreased in larger waves. For ω_e^* values above 5, the heave motions approach zero for all wave heights tested as expected, but more slowly in larger waves.

The dimensionless pitch RAOs (Figure 10) show an increasing dimensionless pitch P^*, from 0.9 to a maximum of 1.1 for all wave heights in the frequency range ω_e^* of 1.9 to 3.1. A maximum P^* of 1.1 was found at ω_e^* of 3.1. For ω_e^* values above 3.1 it can be seen that as the pitch motions reduced with increasing frequency, larger pitch motions were observed to occur during tests in smaller waves.

4. HYDROELASTIC LOADS DATA ANALYSIS

The data obtained for the towing tank tests performed in regular seas was analysed using Excel spreadsheets to determine the strain gauge signal response of the centre bow and demihull elastic hinges as a function of the wave height and wave frequency. This relatively simple approach to the analysis of the unsteady time records was possible because the records of encounter with all waves during a tank run were effectively identical apart from the first one or two wave encounters which were usually rather more severe. It was found that the presence of slam impulse loads and whipping vibratory response was evident in all test conditions where slamming occurred and that the occurrence and severity of slamming in regular waves was dependent upon the wave height and wave frequency.

At low wave encounter frequencies the segmented catamaran model loads were found to be dominated by global wave loads without centre bow slamming. In the absence of slamming, the centre bow was entering and exiting the water without the centre bow arches filling. However at higher encounter frequencies slamming was evident and the impulsive slam load applied to the bow was transmitted dynamically through the bow mounting hinges and to the demihull elastic hinges, producing very much higher peak demihull bending moments than the underlying global wave load during non-slam conditions. The impulsive slam loads applied to the bow caused excitation of the first longitudinal whipping mode of the model as demonstrated by a number of whipping cycles observed in the demihull responses. Figures 11 and 12 show the data from the centre bow and demihull elastic hinges during regular seas tests in 90mm waves at at a dimensionless wave encounter frequency of 4.74. Figure 13 shows an instantaneous photograph captured at these test conditions.

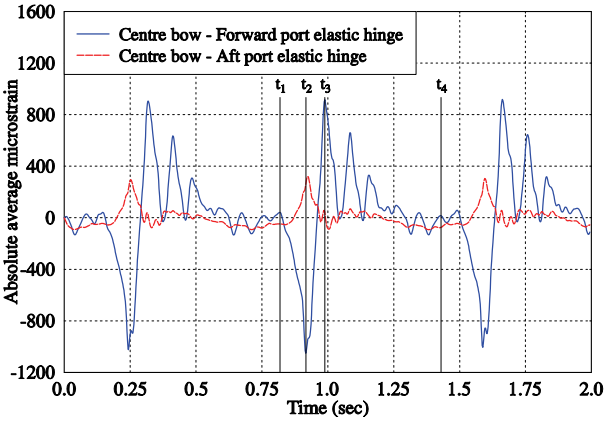

Figure 11: Centre bow raw strain gauge data obtained at a model test speed of 1.53m/s, 90mm wave height and ω_e^* = 4.74 (low-pass filtered at 30Hz).

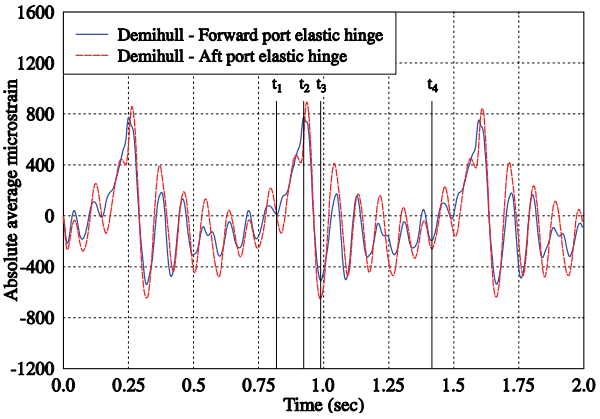

Figure 12: Demihull raw strain gauge data obtained at a model test speed of 1.53m/s, 90mm wave height and ω_e^* = 4.74 (low-pass filtered at 30Hz).

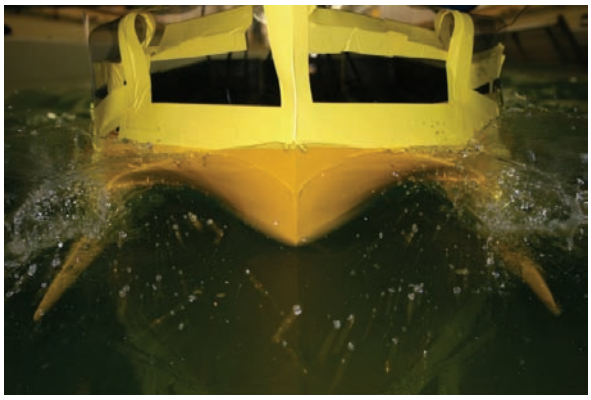

Figure 13: Slamming on the centre bow of the segmented catamaran model at a test speed of 1.53m/s, wave height of 90mm and ω_e^* = 4.94.

We see that the impulse applied to the bow during wave slamming was clearly identifiable in the strain gauge records acquired from the centre bow elastic hinges as shown by the rapid rate of change of strain signals in Figures 11 and 12. The wave slam impulse commenced at time t_1 and achieved a peak sagging response at time t_2 with the peak hogging response observed at time t_3. The whipping vibratory responses occur between time t_3 and time t_4. It was found that the slamming and whipping vibratory responses of the hydroelastic model remained generally similar to those illustrated here for all slam data obtained during these model tests in regular seas. Moreover, the slam signals presented show a slamming and whipping vibration response generally similar to that of the full-scale catamaran vessels [4]. The unsteady bending moments measured at full-scale using strain gauges mounted on the keel of a catamaran vessel [11] were found to be well simulated in respect of the general form of the responses at model scale when compared to the demihull strain gauge full-scale response signals.

5. DYNAMIC STRUCTURAL LOADS

The loads data obtained during the towing tank tests were analysed to determine the magnitude of the maximum slam force acting on the centre bow and the maximum slam induced bending moments acting in the demihull for each wave height and encounter frequency condition. The raw strain gauge signals acquired from the centre bow elastic hinges and the demihull elastic hinges were used to calculate the bending moments measured on the catamaran model. The strains measured on the centre bow elastic hinge mountings were converted to bending moments and used to calculate the slam force acting on the centre bow as described in the preceding section.

The results for the slam force acting on the centre bow as a function of time in a typical test are shown in

Figure 14 at a speed of 1.53m/s and wave height of 90mm at $\omega_e^* = 4.74$.

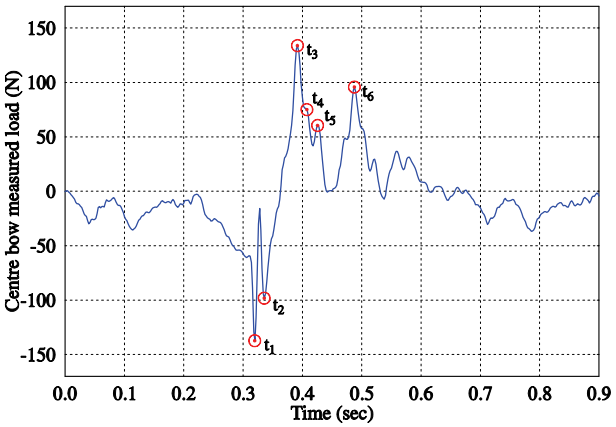

Figure 14: Slam force measured on the centre bow of the catamaran model at a test speed of 1.53m/s, 90mm wave height and $\omega_e^* = 4.74$ (raw data unfiltered).

It can be seen from Figure 14 that the centre bow slam force shows a similar signal waveform to the centre bow strain gauge data presented in Figure 11 as would be expected, although the results shown in Figure 14 depend on the time records for the bending moments in both forward and aft bow mounting transverse beams. In Figure 14 the peak sagging force acting on the centre bow of the model is identified at time t_1 corresponding to the peak sagging strain measured in the centre bow elastic hinges at time t_2 in Figure 11. The peak hogging force acting on the centre bow in Figure 14 was identified at time t_3 corresponding to the peak hogging strain identified at time t_3 in Figure 11. The term 'sagging force' is used here to designate the upward force from the initial slam impact, which generally produces a sagging moment in the demihulls occurring at t_1 in Figure 14. The term 'hogging force' is the force recorded as the centre bow rebounds after the slam impact, at t_3 in Figure 14, generally causing a hogging moment in the demihulls as the centre bow emerges from the immersed state. It is evident that there is a significant hogging force required to extract the bow from the immersed condition.

The whipping vibratory responses identified in the demihull of the catamaran model were also observed in the centre bow slam force data presented in Figure 14, occurring between times t_3 and t_6. However, these whipping dynamic effects on the centre bow are relatively small compared to the main peak loads due to the slam event. Further moderate dynamic vibratory effects are also observed in Figure 14 between times t_1 and t_2 and between times t_4 and t_5. These correspond in time scale (about 0.017 seconds) to the natural frequency of the forward transverse beams measured at a frequency of 60Hz and are relatively small compared to the main slam loads [21].

Analysis of the whole data set for the tank tests showed that wave slamming and whipping did not occur at wave heights of 30mm and 40mm. This result confirms the observations made during full-scale trials performed on a 96m high-speed wave piercer catamaran where wave slamming was not reported to occur at full-scale wave heights below 2m (or 45mm at model scale) as discussed by Thomas [4]. The hydroelastic model tests thus confirmed that increases in the wave height beyond 45mm to 60mm lead to the onset of wave slam with continuing and more severe wave slamming being observed at 90mm and 120mm wave heights.

The wave slam data was finally analysed to evaluate the peak sagging and peak hogging bending loads acting on the demihull and the peak sagging and hogging loads acting on the centre bow of the catamaran model. The peak sagging and peak hogging demihull bending moments and centre bow slam loads were calculated based on the average of the maximum and minimum peak sagging and peak hogging slam loads for all cycles of wave encounter for each model test run. The results will be discussed in the following sections.

5.1 CENTRE BOW PEAK SLAMMING LOADS

The slam loads were evaluated as a function of wave height and wave frequency to demonstrate the parameters affecting the non-linear dynamic wave loads acting on the centre bow. Figure 15 shows the test results for the centre bow peak slam load as a function of wave height and dimensionless wave encounter frequency at a model test speed of 1.53m/s. The left hand ordinate is the peak slam force and the right hand ordinate is the dimensionless peak slam force, *F/mg*, where *F* is the maximum slam force, *m* is the mass of the model and *g* is the acceleration due to gravity.

It can be seen from Figure 15 that the maximum peak sagging slam load measured on the bow was 23.75 kg at a test speed of 1.53m/s and wave height of 120mm at $\omega_e^* = 4.13$. This result showed that the peak slam load measured on the bow corresponded to 87% of the total weight of the model at this test condition. This is consistent with the peak slam loads measured during full-scale vessel trials [12] where the peak slam load was found to reach 93% of the total weight of the vessel. It is further observed that increases in the wave height resulted in increases in the magnitude of the slam load measured on the bow of the catamaran model. At lower wave heights slamming was found to commence at higher encounter frequencies and conclude at lower encounter frequencies when compared to slamming at larger wave heights.

Slamming was found to commence at lower encounter frequencies and conclude at higher encounter frequencies in the larger wave heights. The maximum slam load was found to occur at a rather lower wave encounter frequency at larger wave heights.

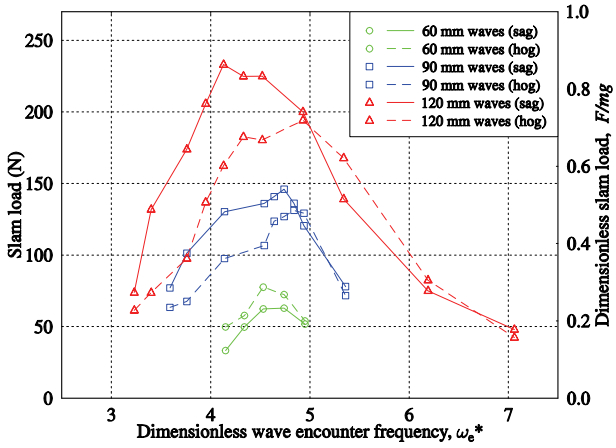

Figure 15: Centre bow peak slam load as a function of wave height and dimensionless wave encounter frequency at a model test speed of 1.53m/s (Fr=0.322).

The proportional increase in the wave loads as a function of wave height is shown more clearly by reducing the centre bow loads data into dimensionless form as a function of the wave amplitude squared. Figure 16 shows the dimensionless slam load acting on the bow as a function of the wave amplitude squared, $F/\rho gL\zeta^2$, where F is the slam force, ρ is the density of water, g is the acceleration due to gravity, L is the overall length of the model and ζ is the wave amplitude. It is observed from Figure 16 that as the wave height is doubled the dimensionless peak sagging slam force maintained almost the same peak value of about 2.7. This shows that the peak sagging slam force was relatively closely related to the square of the wave amplitude.

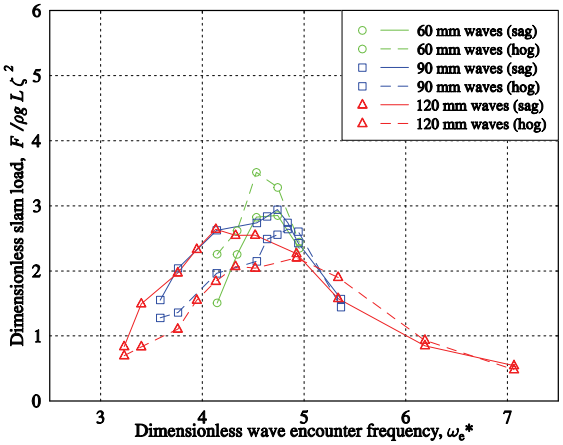

Figure 16: Centre bow dimensionless peak slam load, $F/\rho gL\zeta^2$, as a function of wave height and dimensionless wave encounter frequency at a model test speed of 1.53m/s (Fr=0.322).

5.2 CENTRE BOW SLAM FORCE POSITION

The slam force positions were calculated on the basis of the moments measured on the centre bow transverse beam elastic hinges as discussed earlier. Figure 17 shows the results of the position of the slam force (with reference to the catamaran model demihull transom) as a function of wave height and wave encounter frequency at a model test speed of 1.53m/s.

Increases in the wave frequency caused the position of the slam force to move only slightly further aft while increases in the wave height caused the position of the slam to move further forward. Larger waves were found to produce a peak sagging slam force that was located within the arch of the centre bow and smaller waves were found to produce a peak sagging slam force that was located more aft towards the flat wet-deck section behind the center bow transom. At a model test speed of 1.53m/s the position of the peak sagging slam load was generally found to be forward of the flat wet-deck section. The peak hogging loads were found to act further aft than the peak sagging loads demonstrating the dynamic movement of the wave load during the slamming response, the sag condition preceding the hog condition as the wave surface moves aft.

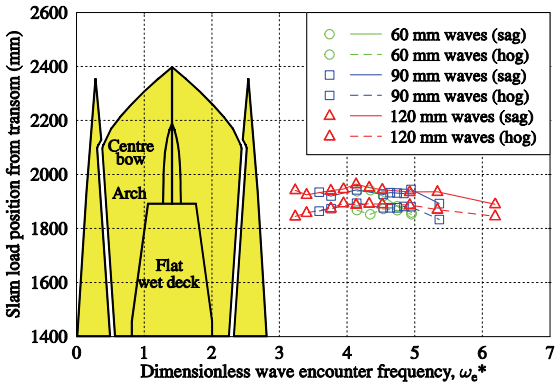

Figure 17: Centre bow peak slam load position forward from the transom as a function of wave height and dimensionless wave encounter frequency at a model test speed of 1.53m/s.

5.3 DEMIHULL SLAM INDUCED BENDING MOMENTS

The slam induced bending moments in the demihulls showed a similar behavior to the slam loads measured on the bow. Figures 18 and 19 show the slam induced bending moments measured in the forward and aft segments respectively of the segmented model during tests performed at a model speed of 1.53 m/ s. The left vertical axis gives the peak slam induced bending moment and the right vertical axis gives the same quantity expressed non-dimensionally, *M/mgL,* where

M is the bending moment, m is the model mass, g is the gravitational acceleration and L is the model length. The bending moment shown in Figure 18 for the forward segment was the summation of the bending moment measured at the forward port and forward starboard elastic hinges and the bending moment presented in Figure 19 for the aft segment was the summation of the bending moment measured at the aft port and aft starboard elastic hinges.

The direct relationship between the slam load on the model bow and bending in the demihulls is immediately apparent when comparing the results of the slam induced bending moments (Figures 18 and 19) with the slam load (Figure 15 and 16). It is observed that increases in wave height gave rise to similar increases in the slam induced bending moments to the increases in slam loads as discussed earlier. The demihull peak sagging response was on average greater than the peak hogging response for all test cases with the exception for tests performed in 60mm waves at a speed of 1.53m/s and ω_e^* of 4.74 rad/s.

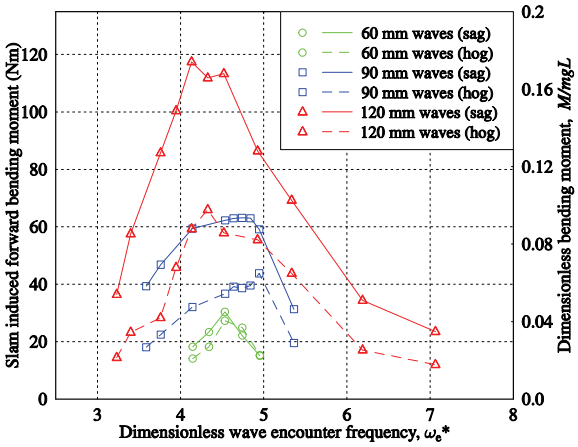

Figure 18: Demihull slam induced peak vertical bending moment at the forward segment position as a function of wave height and ω_e^* at a model test speed of 1.53m/s (Fr = 0.322).

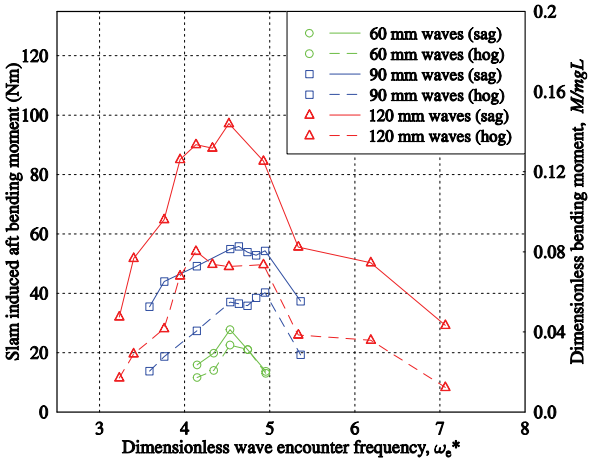

Figure 19: Demihull slam induced peak vertical bending moment at the aft segment position as a function of wave height and ω_e^* at a model test speed of 1.53m/s (Fr = 0.322).

The peak slam induced demihull bending moments were found to coincide with the peak slam loads acting on the centre bow in particular at the forward demihull segment link of the catamaran model. This result demonstrates the direct relationship between the slam load and the bending moments measured in the demihulls. The difference between sag and hog results emphasise the importance of developing numerical techniques to predict the non-linear dynamic structural loads [22]. The strain energy due to the impact of the slam load at the bow produced greater bending moments in the forward segments of the model in comparison to the aft segments [21]. This demonstrates the significance of the dynamic transmission of the slam load through the structure of the model.

The effect of wave height on the slam induced demihull bending moment is also evident in these test results. At a wave height of 60mm peak slam induced bending moments in the forward and aft segments of the model were similar in magnitude. However, an increase of the wave height to 90mm gave rise to a relatively larger increase in the bending moments in the forward segments of the catamaran model compared to the aft segments. It is evident that there are significant non-linear and dynamic effects in both the impulsive wave loading and in the structural response to that loading.

The demihull bending moments were non-dimensionalised using the square of the wave amplitude to gain a clearer understanding of the relationship between the slam induced bending moments and the incident wave amplitude. Figures 20 and 21 show the non-dimensional slam induced bending moments, $M/\rho g L^2 \zeta^2$, where M is the bending moment, ρ is the density of water, g is the gravitational acceleration, L is the ship length and ζ is the wave amplitude. It is observed from Figures 20 and 21 that the maximum value of this parameter is less variable over the range of wave height than was the dimensional moment of Figures 18 and 19. Whereas the moment increased by a factor of about 3.6 for a doubling of the wave height, the dimensionless bending moment remained almost constant at about 0.53. This indicates that the peak sagging bending moments varied approximately with the square of the wave amplitude. The dimensionless peak sagging slam force results presented in Figure 16 thus show a similar variation with the square of the wave amplitude as do the values of the dimensionless peak sagging bending moments shown in Figures 20 and 21. It is also seen from Figure 20 when compared to Figure 21 that the peak sagging slam force caused a greater increase in the dimensionless peak sagging bending moments at the forward segment position when compared to the aft segment position. Further, the dimensionless peak sagging slam forces occur at closely similar wave encounter frequencies to the

dimensionless peak sagging bending moments (comparing Figure 16 to Figures 20 and 21).

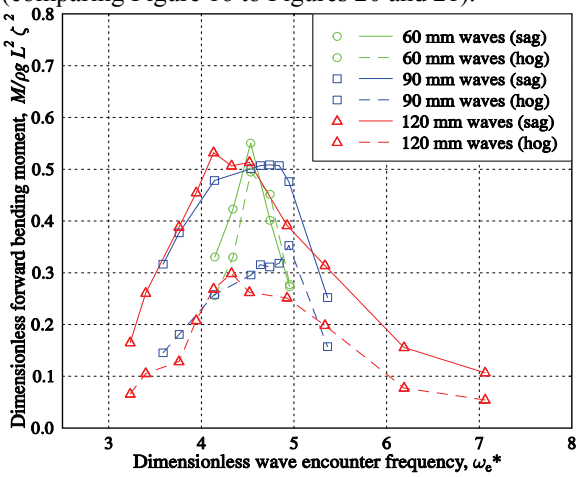

Figure 20: Demihull dimensionless slam induced peak bending moment, $M/\rho g L^2 \zeta^2$, at the forward position as a function of wave height and ω_e^* at a speed of 1.53m/s (Fr = 0.322).

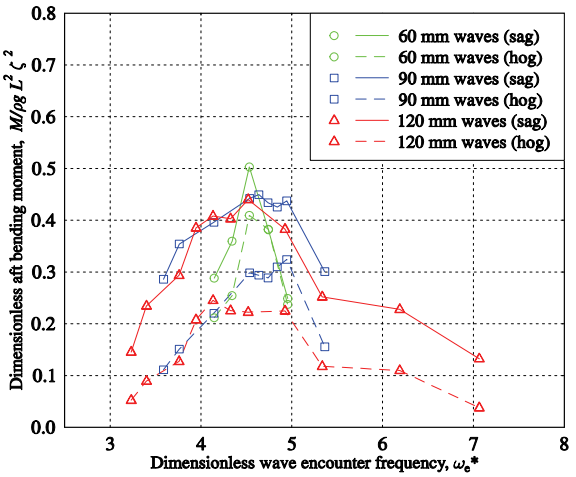

Figure 21: Demihull dimensionless slam induced peak bending moment, $M/\rho g L^2 \zeta^2$, at the aft position as a function of wave height and ω_e^* at a speed of 1.53m/s (Fr = 0.322).

6. SUMMARY OF PEAK DYNAMIC STRUCTURAL LOADS AND HULL MOTIONS

The peak dynamic slam forces of Figure 15 and the peak dimensionless heave and dimensionless pitch results shown in Figures 9 and 10 are summarised in Table 2. In each of the test cases presented it was found that the peak slam loads occurred at significantly higher wave encounter frequencies than the peak heave and peak pitch motions. Thus it appears that there is not a direct relationship between maximum hull motions and maximum slam loadings. However, there are of course still significant hull motions at the dimensionless wave encounter frequencies corresponding to the peak loads.

This implies that the impulsive slam forces are more directly related to the position of the bow relative to the incident wave profile as a result of the wave encounter process [21]. This indicated that the peak slam loads acting on the catamaran model in regular seas were not simply a direct result of the peak heave and pitch motions of the hull. The dimensionless heave and pitch accelerations derived from the dimensionless heave and pitch results are shown in Figures 22 and 23 at a model test speed of 1.53m/s.

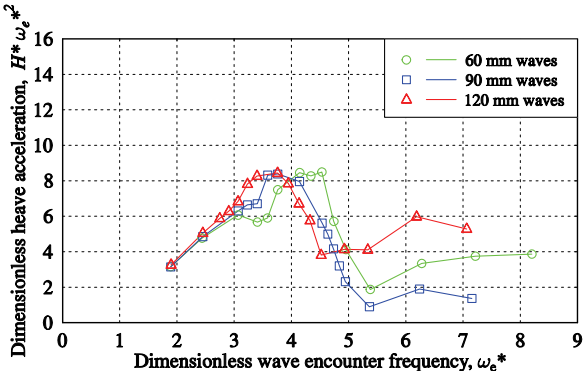

Figure 22: Hydroelastic segmented catamaran model dimensionless heave acceleration, $H^* \omega_e^{*2}$.

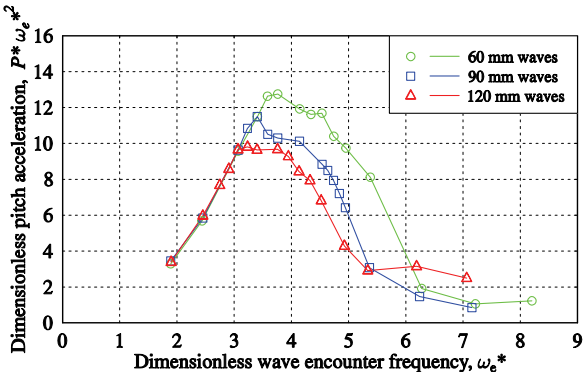

Figure 23: Hydroelastic segmented catamaran model dimensionless pitch acceleration, $P^* \omega_e^{*2}$.

It is seen that the peak dimensionless accelerations occur at dimensionless wave encounter frequencies relatively close to the frequencies at which the peak dynamic slam forces were observed, as shown in Figure 15. We also see from these results that increases in the wave height produced a reduction in the dimensionless accelerations but an increase in dynamic structural loads. Thus, whilst it is difficult to establish a precise association between hull accelerations and slam loads, an indirect association in terms of the frequency of occurrence can be identified. Large accelerations are a consequence of large unsteady forces acting on the hull which themselves must result from large displacements of the hull in the encountered waves. These larger displacements relative to the encountered wave in turn establish the basis for the occurrence of slamming. Thus, it is to be expected that the peak accelerations derived from the hull motions will bear at least a general relationship with the peak dynamic slam forces.

Table 2: Peak values of dimensionless heave, pitch and sagging slam force identified at wave heights of 60mm, 90mm and 120mm at a model test speed of 1.53m/s.

	Wave height								
	60mm			**90mm**			**120mm**		
	H*	***P****	***F* (N)**	***H****	***P****	***F* (N)**	***H****	***P****	***F* (N)**
	0.87	1.01	62.78	0.88	1.04	147.36	0.91	1.03	230.65
ω_e^*	1.89	3.07	4.53	1.89	3.23	4.74	1.90	3.07	4.14

7. CONCLUSIONS

The parameters affecting the slamming responses of a hydroelastic segmented catamaran model during towing tank tests performed in regular seas have been investigated. Strain gauge data obtained from the centre bow and demihull of the catamaran model was analysed to investigate the slam phenomena. It was found that hydroelastic slamming is dependent upon wave height and wave encounter frequency and was identified to commence at wave heights above 60mm for a 2.5m length model. Significant increases in strain were identified in both the centre bow and demihull in the presence of slamming when compared to non-slam regular wave conditions. Slam impulses applied to the bow of the model were found to excite the first longitudinal bending mode of the catamaran model.

Whipping vibration responses observed in the demihull of the catamaran model were evident during all wet-deck slam events. The slamming and whipping vibratory response signal characteristics remained generally similar over all the model tests performed in regular seas and were similar to the results of full scale trials**.** Slamming was found to commence at a higher frequency and cease at a lower frequency in smaller waves while it was found to commence at a lower frequency and cease at a higher frequency in larger waves. The maximum peak sagging slam load measured on the centre bow of the model was found to reach 87% of the total model weight during tests in 120mm waves at a speed of 1.53m/s. Increases in the wave height gave rise to significant increases in the peak sagging slam load measured on the bow of the catamaran model. The peak sagging slam load and slam induced bending moments were found to be approximately proportional to the square of the wave amplitude. The position of the peak sagging slam load acting on the bow of the model was found to be only moderately dependent on wave height and wave encounter frequency and was found to act at a slightly more forward position on the bow in larger waves and at a more aft position on the bow in smaller waves. Increases in the wave encounter frequency caused the position of the peak sagging slam force to move further aft. However, in all cases the slam load acted close to the aft end of the centre bow.

An analysis of the dimensionless heave and dimensionless pitch responses demonstrated that the maximum dimensionless heave and pitch accelerations most closely coincided with the peak dynamic structural loads. It was concluded that high accelerations are associated with large underlying wave loads which themselves are a consequence of large relative motions. These large relative motions form the basis of slamming, so that global accelerations are thus linked to the occurrence and severity of slamming.

8. ACKNOWLEDGEMENTS

This research was undertaken with the support of the University of Tasmania, the Australian Maritime College, Revolution Design, INCAT Tasmania and the Australian Research Council. The work of Shinsuke Matsubara in the design and development of the model is also acknowledged.

9. REFERENCES

1. Dessi, D., De Luca, M., Mariani, R., Correlation of Model Scale and Full-scale Analysis of the Ship Elastic Response in Waves, *Hydroelasticity in Marine Technology, University of Southampton, pp 151- 160*, 2009.

2. Thomas, G., Davis, M. R., Holloway, D. S., Roberts, T. J., The Whipping Vibration of Large High-Speed Catamarans, *Transactions of the Royal Institution of Naval Architects, Volume 145 (A4), pp 13-29,* 2003.

3. Kapsenberg, G. K., Van't Veer, A. P., Hackett, J. P., Levadou, M. M. D., Aftbody Slamming and Whipping Loads, *Transactions of the Society of Naval Architects and Marine Engineers, Volume 111, pp 213–231,* 2003.

4. Thomas, G., Wave Slam Response of Large High-Speed Catamarans. *PhD thesis, University of Tasmania,* 2003.

5. Lewis, E.V. (Ed.), Principles of Naval Architecture, *Society of Naval Architects and Marine Engineers, New Jersey, USA, Volume 1, 2nd edition, pp 208-221*, 1988.

6. Kapsenberg, G. K., Brizzolara, S., Hydroelastic Effects of Bow Flare Slamming on a Fast Monohull, *5th International Conference on Fast Sea Transportation, FAST '99, pp 699–708*, 1999.

7. Belik, O., Bishop, R.E.D., Price, W.G., Influence of Bottom and Flare Slamming on Structural Responses, *Transactions of the Royal Institution of Naval Architects, Volume 129*, *pp 261–276*, 1987.

8. Davis, M. R., Whelan, J. R., Computation of Wet Deck Bow Slam Loads for Catamaran Arched Cross Sections, *Ocean Engineering, Volume 34, pp 2265–2276,* 2007.

9. Holloway, D. S., Davis, M. R., Application of Two Dimensional Boundary Element Methods to Ship Motion Predictions, *Proceedings of the Second International Conference on Computational Fluid Dynamics, pp 375–380,* 2003.

10. Davis, M. R., Holloway, D. S., Validation of Non-linear Wave Loads Predicted by Time Domain Method in Sea Trials of an 86m Catamaran, *8th International Conference on Fast Sea Transportation, FAST '05, pp 375–380,* 2005.

11. Thomas, G., Davis, M. R., Holloway, D. S., Watson, N. L., Roberts, T. J., Slamming Response of a Large High-Speed Wave-Piercer Catamaran, *Marine Technology, Volume 40 (2), pp 126–140,* 2003.

12. Thomas, G., Davis, M. R., Roberts, T. J., Transient Dynamic Slam Response of Large High-Speed Catamarans, *7th International Conference on Fast Sea Transportation, FAST '03,* 2003.

13. Davis, M.R., Whelan, J.R., Modelling Wet Deck Bow Slamming of Wave Piercing Catamarans. *Transactions of the Royal Institution of Naval Architects (Part A), International Journal of Maritime Engineering, Volume A3, 42-57,* 2006.

14. Davis, M.R., Whelan, J.R., Computation of Wet Deck Bow Slam Loads for Catamarans, *Ocean Engineering, 34, 2265-2276,* 2007.

15. Faltinsen, O. M., Hydroelastic Slamming, *Marine Science and Technology, Volume 5, pp 49–65,* 2000.

16. Bereznitski, A., Slamming: The Role of Hyroelasticity, *International Shipbuilding Progress, Volume 48 (4), pp 333–351,* 2001.

17. Hermundstad, O. A., Aarsnes, J. V., Moan, T., Hydroelastic Analysis of a High-Speed Catamaran in Regular and Irregular Waves, *4th International Conference on Fast Sea Transportation, FAST'97, pp 1-12,* 1997.

18. Hermundstad, O. A., Aarsnes, J. V., Moan, T., Hydroelastic Analysis of a Flexible Catamaran and Comparison with Experiments, *3rd International Conference on Fast Sea Transportation, FAST '95, pp 487-500,* 1995.

19. McTaggart, K., Datta, I., Stirling, A., Gibson, S., Glen, I., Motions and Loads of a Hydroelastic Frigate Model in Severe Seas, *Transactions of the Society of Naval Architects and Marine Engineers, Volume 105, pp 427-453,* 1997

20. Lavroff, J., Davis, M. R., Holloway, D. S., Thomas, G., The Vibratory Response of High Speed Catamarans to Slamming Investigated by Hydroelastic Segmented Model Experiments, *Transactions of the Royal Institution of Naval Architects, Volume 151 pp 1–12*, 2010.

21. Dessi, D., Mariani, R., Coppottelli, G., Experimental Investigation of the Bending Vibrations of a Fast Vessel, *Australian Journal of Mechanical Engineering, Volume 4(2), pp 125–144,* 2007.

22. Hermundstad, O. A., Aarsnes, J. V., Moan, T., Linear Hydroelastic Analysis of High-Speed Catamarans and Monohulls, *Journal of Ship Research, Volume 43 (1), pp 48-63,* 1999.

23. Lavroff, J., The Slamming and Whipping Vibratory Response of a Hydroelastic Segmented Catamaran Model. *PhD thesis, University of Tasmania,* 2009.

24. Holloway, D. S., Davis, M. R, Thomas, G., Rigid Body Dynamic Hull Bending Moments, Shear Forces and PCM in Fast Catamarans, *7th International Conference on Fast Sea Transportation, FAST '03, pp B57–B64*, 2003.

